 CMC, vol.18, no.1, pp.69-103, 2010

Simulation of Dendritic Growth with Different Orientation by Using the Point Automata Method

A.Z. Lorbiecka[1] **and B. Šarler**[1,2]

Abstract: The aim of this paper is simulation of thermally induced liquid-solid dendritic growth in two dimensions by a coupled deterministic continuum mechanics heat transfer model and a stochastic localized phase change kinetics model that takes into account the undercooling, curvature, kinetic and thermodynamic anisotropy. The stochastic model receives temperature information from the deterministic model and the deterministic model receives the solid fraction information from the stochastic model. The heat transfer model is solved on a regular grid by the standard explicit Finite Difference Method (FDM). The phase-change kinetics model is solved by the classical Cellular Automata (CA) approach and a novel Point Automata (PA) approach. The PA method was developed and introduced in this paper to circumvent the mesh anisotropy problem, associated with the classical CA method. Dendritic structures are in the CA approach sensitive on the relative angle between the cell structure and the preferential crystal growth direction which is not physical. The CA approach is established on quadratic cells and Neumann neighborhood. The PA approach is established on randomly distributed points and neighbourhood configuration, similar as appears in meshless methods. Both methods provide same results in case of regular PA node arrangements and neighborhood configuration with five points. A comprehensive comparison between both stochastic approaches has been made with respect to curvature calculations, dendrites with different orientations of crystallographic angles and types of the node arrangements randomness. It has been shown that the new method can be used for calculation of the dendrites in any direction.

Keywords: microstructure modeling, solidification, dendritic growth, cellular automata method (CA), point automata method (PA), random node arrangement.

[1] Laboratory for Multiphase Processes, University of Nova Gorica, Slovenia
[2] Corresponding author (B. Šarler) E-mail: bozidar.sarler@ung.si

1 Introduction

Solidification microstructure is very important since it influences the properties of the final casting. Because of that has understanding and modeling of microstructures large industrial relevance. However, the understanding of solidification process and related microstructures is very complicated. This is because it is affected by many interacting phenomena on different scales, such as heat and solute transfer, fluid flow, thermodynamics of interfaces and so on [Rettenmayr and Buchmann (2006)]. Experiments that allow direct visualization of microstructure formation are difficult to perform. In the last decade, several numerical models, which can solve complicated transport phenomena and phase transformation under different boundary and initial conditions, were developed to calculate various microstructure features of solidifying materials such as grain growth with details of solidification interface morphology. Among of all numerical approaches Cellular Automata (CA) modeling [Wolfram (2002)] and phase field modeling [Qin and Wallach (2003)] are the most popular and widely used. We focus on the CA based approach in this paper. A considerable progress on solidification microstructure simulation [Boettinger, Coriell, Greer, Karma, Kurz, Rappaz and Trivedi (2000); Lorbiecka, Vertnik, Gjerkeš, Manojlović, Senčič, Cesar and Šarler (2009); Lorbiecka and Šarler (2010); Miodownik (2002)] has been made by the CA approach.

Rappaz and Gandin [Rappaz and Gandin (1993)] were the pioneering researchers who developed the CA model for modeling microstructure in which nucleation and growth kinetics could be considered and grain structure with certain shapes and size were predicted. Gandin and Rappaz [Gandin and Rappaz (1994); Gandin and Rappaz (1997)] simulated the grain structure by coupling the CA technique for the grain growth with the finite element method (FEM) solver for the heat flow (CA-FEM). Later Spittle and Brown [Spittle and Brown (1995)] coupled the CA with a finite difference solver (CA-FDM) for solute diffusion during the solidification of casting to predict microstructure.

Unfortunately, the simple CA models for dendritic growth suffer from the strong impact of the anisotropy of the numerical grid. Consequences are that they tend to grow only in the grid direction [Zhan, Wei and Dong (2008)]. It does not matter which crystallographic orientation will be chosen it will always shift the dendrite with respect to the grid axis. During the growth processes of grains the crystallographic orientation axes of different grains have different divergence angles with respect to the coordinate system. In these cases is the growth stage difficult to simulate by the CA method. It is because the configuration of the CA mesh has a direct influence on simulated structure and shape. Anderson [Anderson, Srolovitz and Grest (1984)] and later Spittle and Brown [Spittle and Brown (1989)] used a hexagonal, rather than the standard square 2-D lattice in order to better represent the

grain anisotropy. But in general even now it is still difficult to properly model the preferred crystallographic orientation. Rappaz and Gandin developed a decentered square method [Rappaz and Gandin (1993)] to try to solve this problem, which turns out to be very complicated.

We present a novel Point Automata (PA) method in this paper which follows the CA concept and is able to solve the mentioned crystallographic orientation problem. A basic feature of this method is to distribute nodes randomly in the domain instead of using regular cells, which leads to different distances between the nodes and different neighborhood configurations for each of them. This new approach was first proposed by Janssens for modeling the recrystallisation [Janssens (2000); Janssens (2003); Janssens (2003); Janssens (2010); Raabe, Kozeschnik, Miodownik and Nestler (2007); Janssens]. [Lorbiecka, Vertnik, Gjerkeš, Manojlović, Senčič, Cesar and Šarler (2009)] were the first to couple the classical CA method with a meshless method instead of the FEM or FDM. They succesfully predicted the grain structure in continuous casting of steel. Subsequently, they replaced the CA method by the PA method in the same physical system [Lorbiecka and Šarler (2009)] and demonstrated the suitability of the PA method for cellular to equiaxed and equiaxed to cellular transition simulation in steel billets. The preliminary results of the dendritic growth based on the PA approach have been presented in [Lorbiecka and Šarler (2009)]. This approach is explained and evaluated in details in the present paper where we numerically discuss a simple physical model which can simulate the dendritic forms during the solidification of pure metals from its undercooled melt. The developed algorithm is able to obtain the dendritic morphology by solving the heat transfer equation coupled with the solid fraction field evolution through the calculations of crystal growth velocity, interface curvature, thermodynamic and kinetic anisotropy, respectively.

The present paper is structured in the following way: the CA and the PA methods are defined first, followed by the description of the governing equations of the heat transfer model and the stochastic model. The solution of temperature field and solid fraction is explained afterwards. The differences in numerical implementation of the classical CA and the new PA solution procedure are compared and discussed. The dendritic growth is simulated for ten different orientations with the same random node arrangement with the PA method. Afterwards, the influence of four different random node arrangements as well as different node randomness was tested on two different crystallographic orientations. Finally, the numerical results are shown for the classical CA method with and without fluctuations and compared to the results obtained by the PA method. Conclusions with systematically listed characteristics of the PA method and future developments of the PA method complete the present paper.

2 CA and PA definitions

Numerical models for solving the microstructure equations can briefly be divided into two categories: deterministic and stochastic [Stefanescu (2009)]. Stochastic modeling represents a system where the physical phenomena are described by the random numbers. As a consequence the output data can vary from one simulation to another. The most popular stochastic methods used to simulate the microstructure formations are: Monte Carlo methods, Random Walker and CA approach. CA stochastic method [Wolfram (2002)] represents one of the numerical techniques, widely applied in modeling solidification and recrystallization processes. This algorithm was first established by Neumann [Neumann (1987)] and is nowadays commonly used in material science. What follows are the basic elements of the CA method

- n-D (n=1, 2, 3) space is divided into a discrete number of n-dimensional elements which are named cells (polygons and polyhedrons).
- a state is assigned to each CA cell,
- the neighborhood configuration is defined deterministic or stochastic for each CA cell,
- transition rules are defined which create a new state of the cell as a function of the states(s) of the cell(s) consisting of the previously defined local neighborhood of the cell.

The above presented basic features of the CA system are commonly implemented in the literature. In the present work an alternative formulation to a common CA method is introduced. What follows are the basic elements of this novel PA method

- the starting point is to distribute PA nodes (not cells) randomly on the n-D computational domain,
- a state is assigned to each PA node,
- the neighborhood configuration is defined for each node separately with respect to the chosen neighborhood configuration,
- the neighborhood of the node includes all random nodes whose positions are located in the domain of a circle in 2D or sphere in 3D. The number of the neighbors can vary locally. The transition rules are defined and they create a new state of the point as a function of the states(s) of the points(s) consisting the local neighborhood configuration.

The irregular (also named random) PA cellular transitions rules can be used in exactly the same way as for the regular approach. In this sense the PA approach is not much different from the conventional one, despite bringing many advantages listed in the conclusions.

3 Governing equations

Thermally induced dendrite growth is considered in this paper. It is physically described by the heat conduction and phase change kinetics. The temperature field is solved by the classical deterministic method and the phase change kinetics by the stochastic method.

3.1 Temperature field

Consider a two dimensional domain Ω with boundary Γ filled with a phase change material which consists of at least two phases, solid and liquid, separated by an interfacial region, which is usually very thin in pure substances. The thermal field in such a system is governed by the following equation [Xu, Li, Liu and Liu (2008)]

$$\frac{\partial}{\partial t}(\rho h) = \nabla \cdot (\lambda \nabla T) \tag{1}$$

where ρ, h, λ, T represent material density, specific enthalpy, thermal conductivity and temperature, respectively.

The specific enthalpy is constituted as

$$h = c_p T + f_l L \tag{2}$$

where c_p, L, f_l represent the specific heat, the latent heat and liquid fraction, respectively. All material properties are assumed constant for simulation simplicity. The solid and liquid fractions follow the rules

$$f_s + f_l = 1 \tag{3}$$

$$f_s(T) = \begin{cases} 1 & \text{for } T \leq T_s \\ \frac{T_l - T}{T_l - T_s} & \text{for } T_s < T < T_l \\ 0 & \text{for } T \geq T_l \end{cases} \tag{4}$$

where T_s, T_l, f_s represent the solidus temperature, liquidus temperature and the solid fraction, respectively. In case of pure substance are the solidus and the liquidus temperatures equal to the melting temperature T_m. However, for the computational purposes a narrow melting interval is always present $T_l > T_m > T_s$. The melting temperature T_m is defined as $T_m = \frac{1}{2}(T_s + T_l)$.

We search for the temperature at time $t_0 + \Delta t$ by assuming the initial conditions

$$T(\mathbf{p}, t_0) = T_0(\mathbf{p}); \ \mathbf{p} \in \Omega \tag{5}$$

$$f_s(\mathbf{p}, t_0) = f_{s0}(\mathbf{p}); \ \mathbf{p} \in \Omega \tag{6}$$

(where **p** represents the position vector) and Neumann boundary conditions

$$\frac{\partial T}{\partial n}(\mathbf{p}, t) = F(\mathbf{p}, t); \ \mathbf{p} \in \Gamma, \ t_0 < t \leq t_0 + \Delta t \tag{7}$$

where **n** represents the normal on Γ and T_0, f_{s0},F represent known function.

3.2 Phase change kinetics

3.2.1 Interface undercooling

The phase change situation can be achieved by undercooling a liquid below its melting temperature. When a solid seed is placed in such an undercooled melt, solidification will be initiated. Due to crystal anisotropy and perturbations in the system, the growth of the solid from the seed will not be uniform and an equiaxed dendritic crystal will form. Solid liquid interface is undercooled to the temperature T_f defined as [Saito, Goldbeck-Wood and Muller-Krumbhaar (1988); Nakagawa, Narsume and Ohsasa (2006)]

$$T_f = T_m - \Gamma K \tag{8}$$

where Γ and K are the Gibbs-Thomson coefficient and the interface curvature, respectively.

3.2.2 Dendrite growth kinetics

The growth process is driven by the local undercooling. The interface growth velocity is given by the classical sharp model [Shin and Hong (2002)]

$$V_g^*(p, t) = \mu_K (T_f - T(p, t)); \ p \in \Gamma_{s,l} \tag{9}$$

where V_g^*, μ_K, $\Gamma_{s,l}$ is the growth velocity, interface kinetics coefficient and the solid liquid interface, respectively.

Dendrites always grow in the specific crystallographic orientations. Therefore it is necessary to consider anisotropy in either the interfacial kinetics or surface energy (or both). The present model accounts for the anisotropy in both kinetics.

3.2.3 Thermodynamic anisotropy

The Gibbs-Thomson coefficient can be evaluated [Krane, Johnson and Raghavan (2009)] by taking into account the thermodynamic anisotropy related to the crystal orientation and type as follows

$$\Gamma = \overline{\Gamma}\left[1 - \delta_t \cos\left[S\left(\theta - \theta_{def}\right)\right]\right] \tag{10}$$

where S, θ, θ_{def},δ_t, $\overline{\Gamma}$ represent factors which control the number of preferential directions of the material's anisotropy ($S = 0$ for the isotropic case, $S = 4$ for four fold anisotropy and so on), growth angle (angle between the$y$coordinate and the line that connects the center of the mass of the dendrite and point at $\Gamma_{s,l}$, see Fig. 1), the preferential crystallographic orientation, thermodynamic anisotropy coefficient and the average Gibbs - Thomson coefficient, respectively.

3.2.4 Kinetic anisotropy

The crystal growth velocity is calculated according to the crystal orientation by taking into the consideration the crystal growth direction θ and the preferred orientation θ_{def}. The crystal growth velocity follows the equation [Shin and Hong (2002)]

$$V = V_g^*(p,t)\left[1 + \delta_k \cos\left(S\left(\theta - \theta_{def}\right)\right)\right] \tag{11}$$

where δ_k represents the degree of the kinetic anisotropy, respectively.

3.3 Coupling

The movement of the solid-liquid interface is governed by the evolution of the temperature field in the computational domain (Fig. 1). The dendritic structures are modeled by the stochastic method to track the interface motion coupled to the determinate heat transfer calculations. We first describe the solution of the temperature field based on the FDM method and subsequently the transition rules for the CA (PA) methods for calculation of solid fraction field. The flowchart of the calculations is given in Fig. 18.

4 Solution of the temperature field

A square domain is considered with length l. The number of points in FDM mesh in $x$and$y$directions is N. The total number of FDM grid points is N^2- 4, since the four corner nodes are not considered.

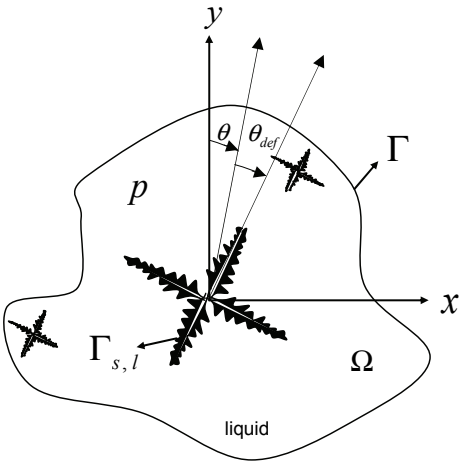

Figure 1: Scheme of the dendrite growth

A uniform FDM discretization is made with mesh distance $\Delta x = \Delta y = a = l/(N-1)$as seen in Fig. 5 (top). The solution for the temperature field is performed by the simple explicit FDM. Solution of the temperature field in the domain nodes is thus

$$T_{i,j} = T_{0\,i,j} + \frac{\Delta t \lambda}{\rho c_p}\left(\left[\left(T_{0\,i-1,j} - 2T_{0\,i,j} + T_{0\,i+1,j}\right)/\left(\Delta x^2\right)\right]\right.$$
$$\left. + \left[\left(T_{0\,i,j-1} - 2T_{0\,i,j} + T_{0\,i,j+1}\right)/\left(\Delta y^2\right)\right]\right) + + \frac{L}{c_p}\left(f_{s\,i,j} - f_{0s\,i,j}\right) \quad (12)$$

for $i = 2,3,...,N-1$ and $j = 2,3,...,N-1$

The boundary nodes are calculated (the Neumann boundary conditions are set to $F = 0\mathrm{W/m}^2$) as

West

$$T_{1,j} = T_{2,j} \quad (13)$$

for $j = 2,...,N-1$

East

$$T_{N,j} = T_{N-1,j} \quad (14)$$

for $j = 2,...,N-1$

North

$$T_{i,N} = T_{i,N-1} \quad (15)$$

for $i = 2, ..., N-1$

South

$$T_{i,1} = T_{i,2} \tag{16}$$

for $i = 2, ..., N-1$

where Δt, $f_{0s\,i,j}$, $T_{0\,i,j}$, $T_{0\,i+1,j}$, $T_{0\,i-1,j}$,$T_{0\,i,j+1}$, $T_{0\,i,j-1}$ are the time step, initial solid fraction, initial temperature in the FDM central, east, west, north and south nodes, respectively.

5 Solution of the solid fraction field

We now define and discuss the elements of the classical CA and the novel PA methods in details.

5.1 Definition of mesh and neighborhood configuration

Square cells with length $\delta x = \Delta y = a = l/n$ where $n = N-1$, represents the number of cells in x and y directions are considering in the CA approach. In the PA approach the square is divided in uniform or nonuniformy distributed nodes. Cells are not defined.

5.1.1 Mesh and neighborhood in the CA method

A basic definition of neighborhood originates from the classical CA approach which operates on the grid divided into the square cells [Neumann (1987); Nastac (2004)]. The cell structure is depicted in Fig. 2. In our calculations the Neumann configuration which takes into account only the closest neighbor's cells during the computation is applied.

The conventional square mesh structure is commonly applied in CA calculations. It represents a square domain covered by the CA cells $x_{CA\,i,j}$, $y_{CA\,i,j}$ located exactly in the middle of four FDM nodes, as it is depicted in Fig. 5 (middle).

$$x_{CA\,i,j} = \frac{1}{2}\left[x_{FDM\,i,j} + x_{FDM\,i+1,j}\right] \tag{17}$$

$$y_{CA\,i,j} = \frac{1}{2}\left[y_{FDM\,i,j} + y_{FDM\,i,j+1}\right] \tag{18}$$

5.1.2 Mesh and neighborhood in the PA method

The PA node grows with respect to the heat flow and with respect to the 'neighbourhood' configuration which is now associated with the position of the neighbouring

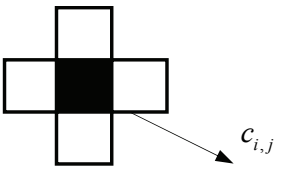

$$c_{i,j} = \left\{ c_{i+1,j}, c_{i,j+1}, c_{i-1,j}, c_{i,j-1} \right\}$$

Figure 2: Graphical representation of the Neumann neighborhood configuration for the conventional CA method

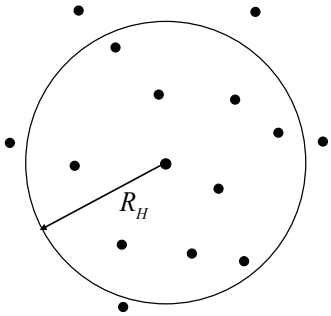

$$c_{i,j} = \left\{ c_{i,j}; \left| r_i - r_j \right|_{i \neq j} < R_H \right\}$$

Figure 3: Graphical representation of the neighborhood configuration proposed for the new PA method

PA nodes which fall into a circle [Janssens (2000); Janssens (2003)] with radius R_H in 2-D or a sphere in 3-D. It means that each PA node can in case of the random mesh contain different number and position of the neighbors, which give various possibilities of neighborhood configurations for each node.

For the novel PA method the random node arrangement is in the present paper generated from the regular CA mesh.

To construct the random node arrangements the CA cell centers are displaced to the randomly chosen positions and become random PA nodes $x_{PA\,i,j}$, $y_{PA\,i,j}$ on the

computational domain (see Fig.5 bottom).

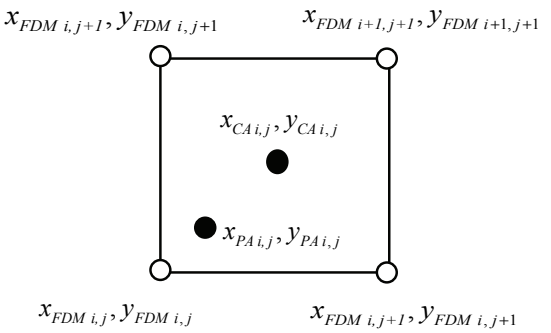

Figure 4: Schematic representation of the relationship between FDM nodes (4 corners), CA cell (center) and the random PA node

The displacement of each CA center is assumed only in the square area appointed by the four FDM nodes. The following procedure is applied

$$x_{PA\ i,j} = x_{CA\ i,j} + \varepsilon\ [2rand - 1] \tag{19}$$

$$y_{PA\ i,j} = y_{CA\ i,j} + \varepsilon\ [2rand - 1] \tag{20}$$

where $x_{PA_{i,j}}$, $y_{PA_{i,j}}$, ε represent coordinates of PA nodes and the scaling value $0 \leq \varepsilon \leq 0.49$, respectively.It must be emphasized that the PA procedure is established on the random nodes in general. The heat transfer calculations are performed on the regular FDM nodes, which is briefly explained in Section 6.

5.2 Curvature calculations

The interface curvature is approximated by the counting cell procedure developed by Sasikumar and Sreenivasan [Sasikumar and Sreenivasan (1994)].

5.2.1 Calculation of curvature in the CA method

The expression for curvature K is given by the formula [Krane, Johnson and Raghavan (2009)]

$$K = \frac{1}{a}\left(1 - \frac{2N_{s\,CA}}{N_{t\,CA}}\right) \tag{21}$$

where $N_{s\,CA}$ and $N_{t\,CA}$ are the number of solid CA cells whose centers fall inside the circle of assumed radius R_c and the total number of CA cells whose centers fall inside the circle, respectively (see Fig. 6).

5.2.2 Calculation of curvature in the PA method

The expression for PA is derived from the expression at the CA method Eq.21 by assuming the average node distance $\overline{a}$ instead of a.

$$K = \frac{1}{\overline{a}} \left(1 - \frac{2N_{s\,PA}}{N_{t\,PA}} \right) \tag{22}$$

where $N_{s\,PA}$, $N_{s\,PA}$ are the number of solid PA nodes inside the circle of assumed radius R_c and the total number of PA nodes inside the circle, respectively (see Fig. 7).

The curvature of both methods has been calculated and compared on a circular solid fraction arrangement with radius $R = 10\,\mu m$, depicted in Fig. 8. Two different types of R_c have been chosen ($R_c = 1\mu m$ and $R_c = 5\mu m$). It can be concluded that with the higher radius R_c the value of K becomes almost the same as in the conventional CA approach. This was depicted in Fig. 9 and Fig. 10, respectively.

5.3 Phase change

The crystal growth velocity is calculated according to the crystal orientation. The envelope of the grain can be expressed by the Eq.11 which is depicted in Fig.11. Once a CA cell (or PA node) becomes solid it starts to grow with respect to the 'neighborhood' configuration (see Fig. 2 and Fig. 3). Each of the CA cell (or the random node) can have two possible states: liquid or solid. The CA cell (or PA node) becomes solid through the growth process. The change of solid fraction of the CA cell or PA node is calculated from the crystal growth velocity.

For all neighbors of the treated solid CA cell (or solid PA node), general criterion d is checked which is represented by the following formula

$$d = \frac{l\,(t)}{a_i} \tag{23}$$

$$l = \int_{t_0}^{t} V_{i,j}\,dt \tag{24}$$

where a_i represent lengths from the analyzed CA cell or PA node to the nearest one.

If neighbor is one of the four nearest east, north, west, south neighbors then in the CA method this distance becomes $a_i = a$. In the PA method $a_i (a_i < R_H)$ represents the different distances to the neighboring PA nodes which fall into the circle with radius R_H (see Fig. 14 and Fig. 15).

When $d \geq a$ or $d \geq a_i$ (Fig. 13 and Fig. 15) the growing solid touches the centre of the neighboring CA cell or PA node and this cell/node transforms its state from liquid to solid $f_{s\,PA} = 1$.

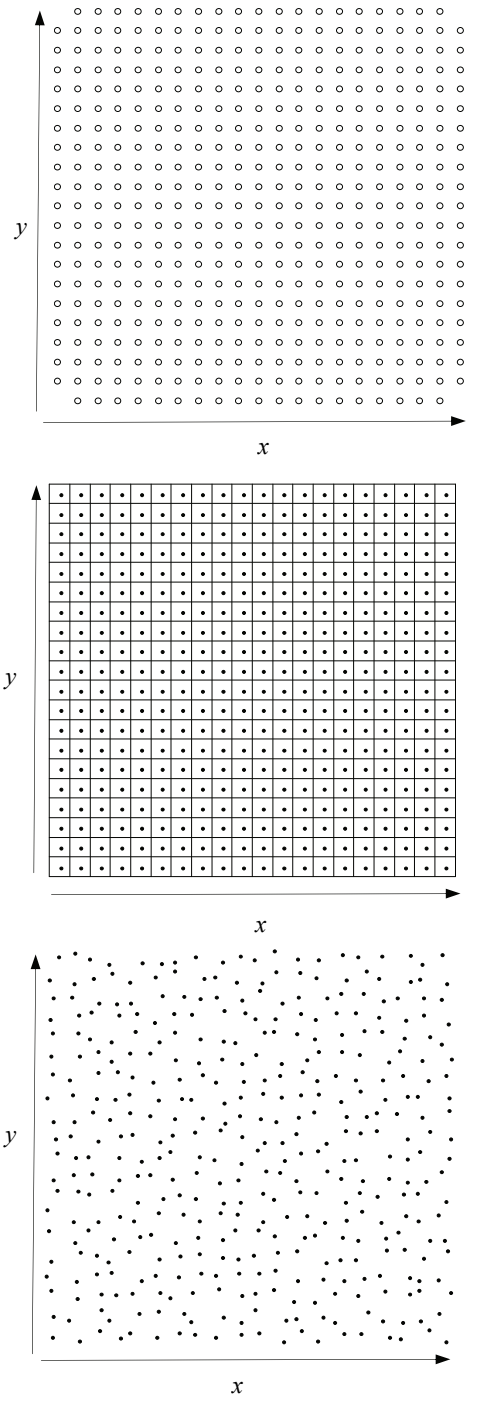

Figure 5: Scheme of space discretization: (top) FDM nodes with $N = 21$, (middle), CA cells with $n = 20$, (bottom) PA nodes with $n = 20$

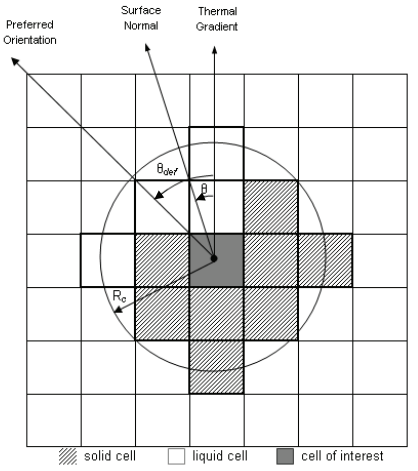

Figure 6: Scheme showing a circle sample with $R_c = 2a$ for calculating the curvature of the conventional CA method (example: $N_{s\,CA} = 8$ and $N_{t\,CA} = 12$)

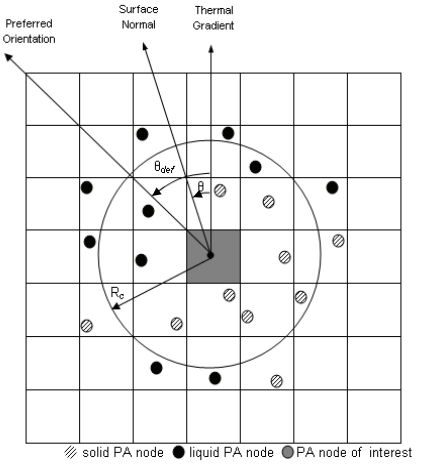

Figure 7: Scheme showing a circle sample with $R_c = 2a$ for calculating the curvature for the random PA nodes (example: $N_{s\,PA} = 7$ and $N_{t\,PA} = 11$)

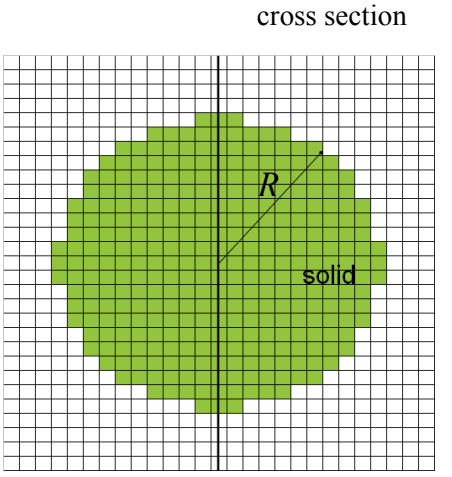

Figure 8: Scheme of the area used to compare the curvature calculations by the CA and PA methods. $R = 10\mu$m. Filled area represents solid

6 FDM-PA-FDM transfer of temperature and solid fraction

6.1 FDM-PA transfer of temperature

The obtained values of temperature on regular FDM grid (see Section 4) are in each time step transferred to random PA grid according to the described scheme (Fig. 18).

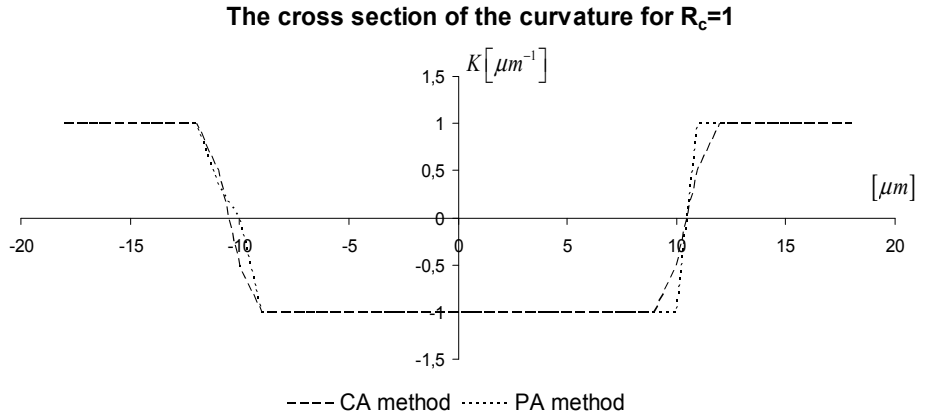

Figure 9: Calculated curvature K with the CA and PA method ($\varepsilon = 0.49$) for $R_c = 1\mu$m and $a = \overline{a} = 1\mu$m with respect to the data depicted in Fig. 8

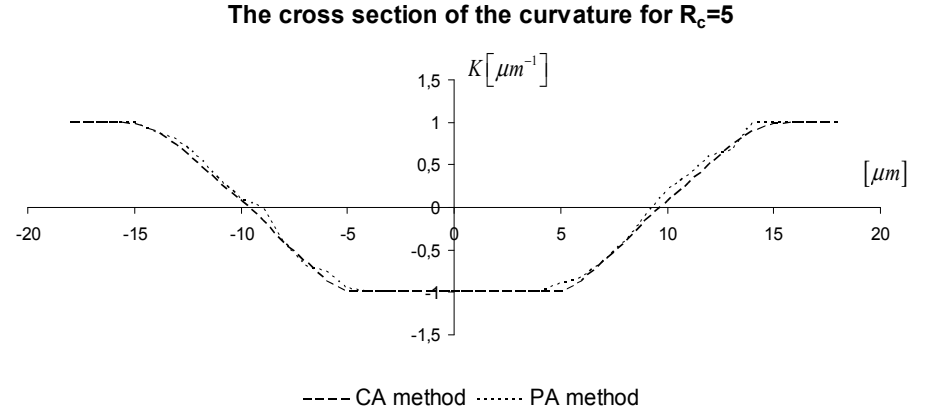

Figure 10: Calculated curvature K with the CA and PA-(A) method for $R_c = 5\mu$m and $a = \overline{a} = 1\mu$m with respect to the data depicted in Fig. 8

The following simple interpolation formula [Xu and Liu (2001)] is used in the present paper

$$T_{PA\,i,j} = \left(T_{i,j+1}l_1 + T_{i+1,j+1}l_2 + T_{i+1,j}l_3 + T_{i,j}l_4\right) / \sum_{i=1}^{4} l_i \tag{25}$$

In case of FDM-CA the Eq.25 reduces to

$$T_{CA\,i,j} = \left(T_{i,j+1} + T_{i+1,j+1} + T_{i+1,j} + T_{i,j}\right)/4 \tag{26}$$

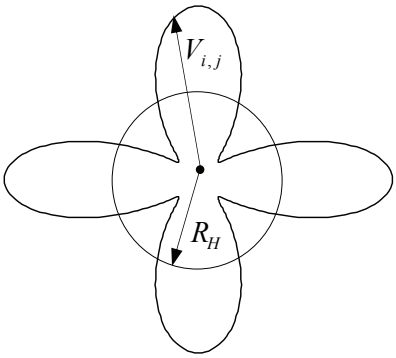

Figure 11: Schematic representation of the shape function (parameters see Tab.1)

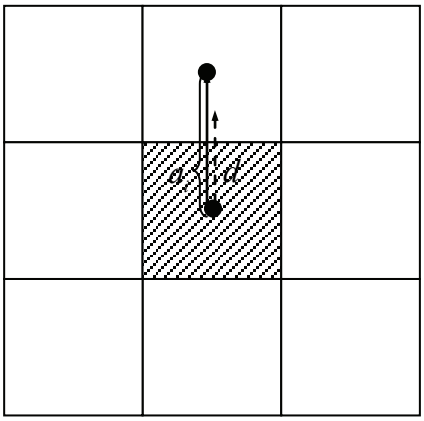

Figure 12: Growth front will not reach the closest neighbor $d < a_i$. The CA cell will not be converted to solid (example for the Neumann neighborhood configuration)

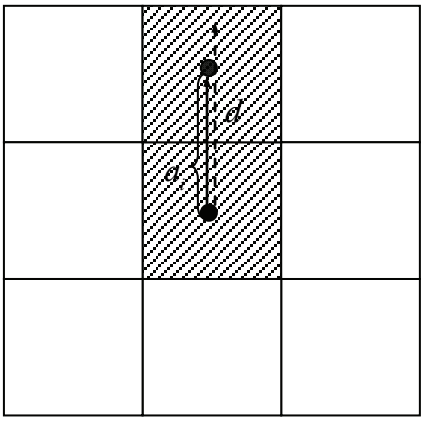

Figure 13: Growth front will reach the closest neighbor$d \geq a_i$. The CA cell will be converted to solid (example for the Neumann neighborhood configuration)

where $T_{PA\,i,j}$, $T_{i,j}$, $T_{CA\,i,j}$ and l_i represent the temperature of the PA node, the temperatures of the four closest FDM nodes, the temperature for the center CA cell and the distances to the nearest four FDM nodes, respectively. The calculation is repeated in each time step (see Fig. 16).

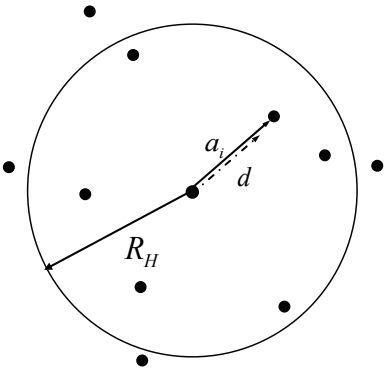

Figure 14: Growth front will not reach the closest neighbor $d < a_i$. The PA node will not be converted to solid

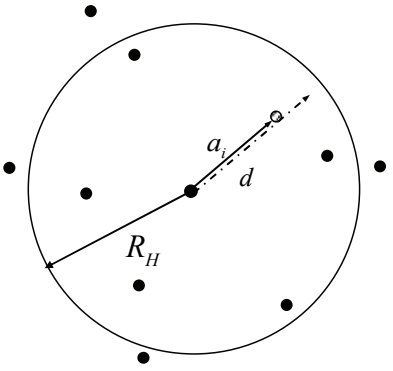

Figure 15: Growth front will reach the closest neighbor $d \geq a_i$. The PA node will be converted to solid

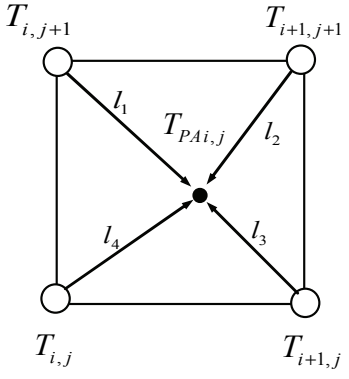

Figure 16: Relationship between four FDM nodes and PA node for the calculation of the temperature values

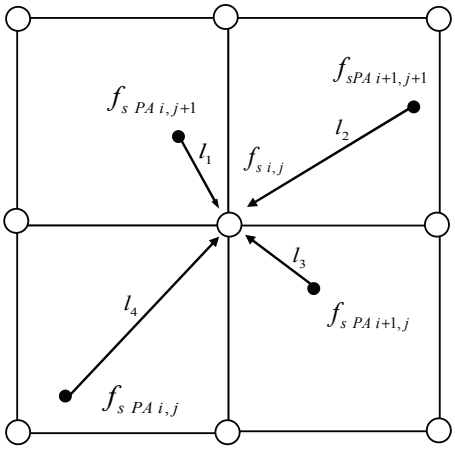

Figure 17: Relationship between the FDM node and four neighboring PA nodes for the transfer of solid fraction

6.2 PA-FDM transfer of solid fraction

The temperature field at time $t_0 + \Delta t$ can be calculated from the Eq.12 for all FDM nodes. Then these values are recalculated to all PA nodes according to the Eq.25. Afterwards the PA procedure takes place (see Section 3). The output information from this level of calculation is the value of solid fraction for all random PA nodes

$f_{s\,PA\,i,j}$ which have to be transferred to the FDM nodes to be able to calculate the new values of temperature (Fig. 17). The following equation is applied

$$f_{s\,i,j} = (f_{s\,PA\,i,j+1}\,l_1 + f_{s\,PA\,i+1,j+1}\,l_2 + f_{s\,PA\,i+1,j}\,l_3 + f_{s\,PA\,i,j}\,l_4)/\sum_{i=1}^{4} l_i \tag{27}$$

In case of FDM-CA the Eq.27 reduces to

$$f_{s\,i,j} = (f_{s\,CA\,i,j+1} + f_{s\,CA\,i+1,j+1} + f_{s\,CA\,i+1,j} + f_{s\,CA\,i,j})/4 \tag{28}$$

where $f_{s\,i,j}$ and $f_{s\,PA}$ represent the solid fraction for the FDM nodes and for the PA nodes, respectively.

7 Numerical example

7.1 Numerical implementation

The model was coded in Fortran. For the dendritic growth in Fig.20 the CPU time varies from 10 to 15 minutes depending on the input data. The solid PA node or CA cell are depicted by colored pixel which can be observed on the screen during the simulation.

7.2 Problem definition and discretization

Initial conditions. Simplified material properties presented in Tab. 1 for pure aluminum [Kammer (1999)] are used in all prepared numerical examples. The process starts from the predetermined solid seed position in one single PA or CA node in the middle of the computational domain with the following initial conditions of temperature $933.45\,K - 1.5\,K$ and solid fraction $f_s = 1$.

All other PA nodes are assumed to be liquid $f_s = 0$ and FDM nodes with the temperature $770.23\,K$. This data is constant with the problem defined in the article. The numerical examples in the present paper are solved by the FDM based temperature calculations and CA or PA based solid fraction calculations. The computational domain of the square with $l = 350\,\mu m$ in uniform discretization $N = 701$.

Mesh generation. FDM and CA methods are always constructed on a regular node arrangement in the present paper. In the PA approach the random node arrangement needs to be constructed. The PA approach was tested first with the predetermined node arrangement PA-(A), see Fig. 20 and then with different types of random node arrangements: PA-(B), PA-(C), PA-(D), see Figs. 21-23, respectively (Tab.2).

Time step. The time step used in FDM calculation of the temperature field is limited by the formula [Zhu and Hong (2001)]

$$\Delta t_{FDM} = \frac{a^2}{4.5D};\; D = \frac{\lambda}{\rho c_p} \tag{29}$$

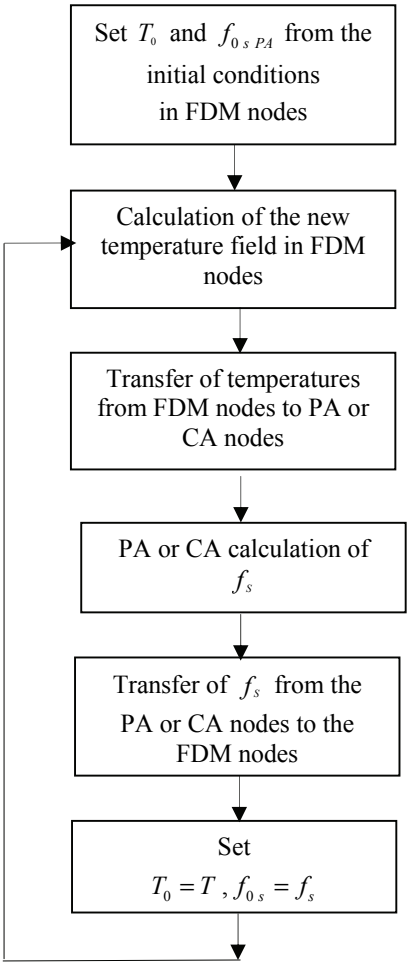

Figure 18: Flowchart of the thermal field and solid fraction calculations

where D represents the thermal diffusivity. For the calculations of the solid fraction field by the CA and PA method the following relation is used [Daming, Ruo and Zhang (2004)] for assuming stability

$$\Delta t_{CA} = \eta \min\left(\frac{a}{V^*_{\max}}, \frac{a^2}{D}\right) \tag{30}$$

where η and $V^*_{\max}$ represent the positive constant less then 1 and the maximum growth velocity of all interface cells, respectively.

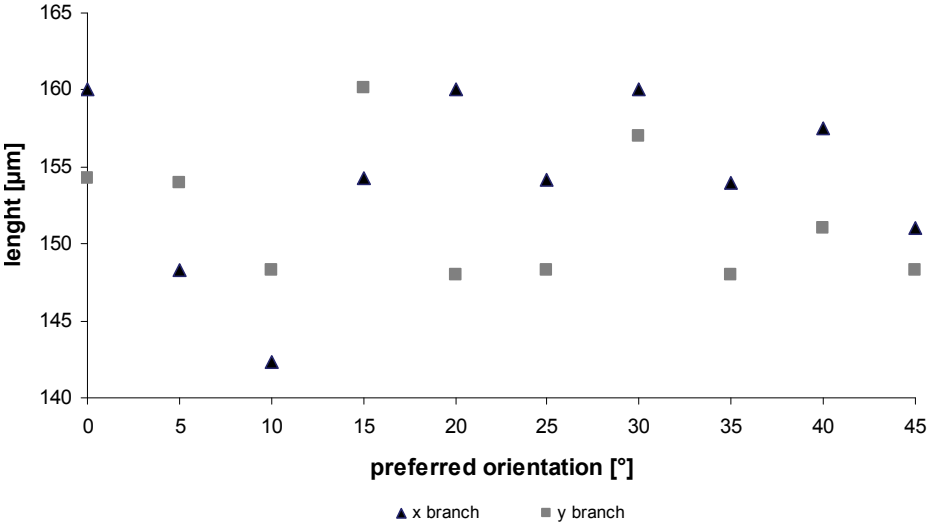

Figure 19: The lengths of dendrite branches in x and y directions for ten different crystallographic orientations, random node arrangement PA-(A), (see Fig.20)

For the stability of the coupled FDM-CA-PA procedure a minimum of Δt_{CA} and Δt_{FDM} should be used. All depicted results of simulations are shown for the different crystallographic angles after 1500 time steps of the length $\Delta t_{FDM} = 6.82 \times 10^{-10}$s.

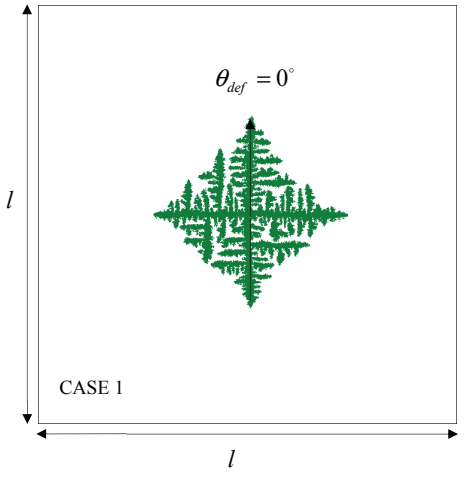

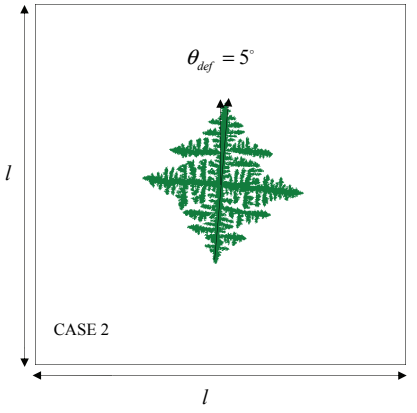
$\theta_{def} = 5^{\circ}$
CASE 2
l
l

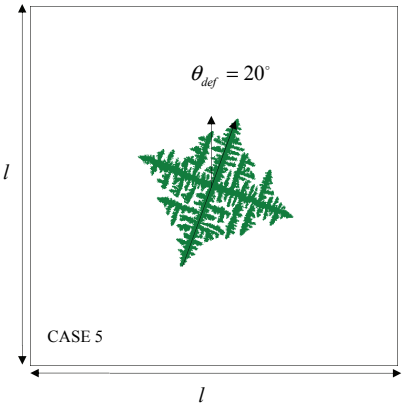
$\theta_{def} = 20^{\circ}$
CASE 5
l
l

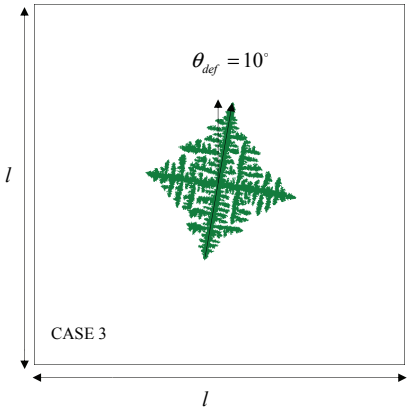
$\theta_{def} = 10^{\circ}$
CASE 3
l
l

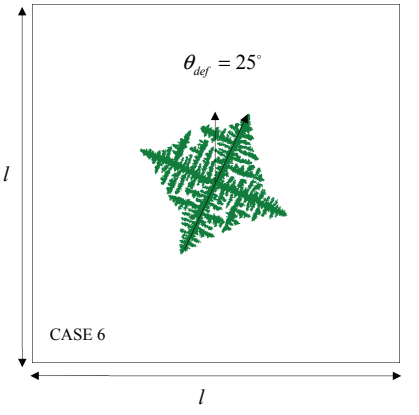
$\theta_{def} = 25^{\circ}$
CASE 6
l
l

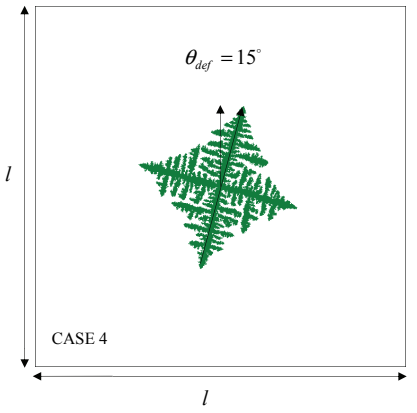
$\theta_{def} = 15^{\circ}$
CASE 4
l
l

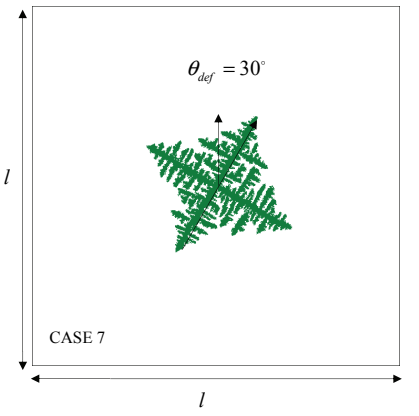
$\theta_{def} = 30^{\circ}$
CASE 7
l
l

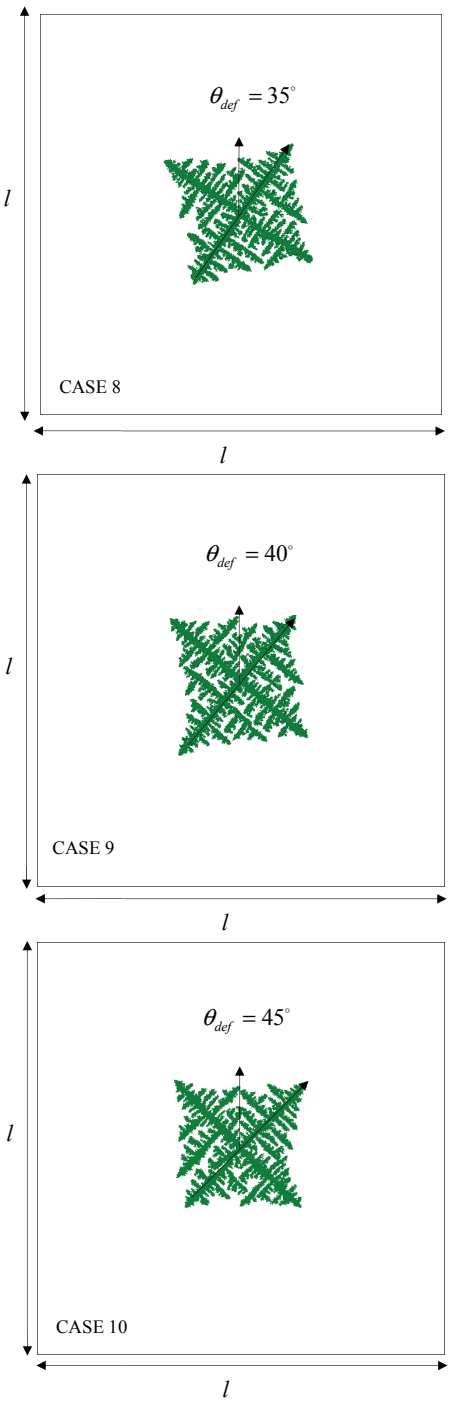

Figure 20: Simulated dendritic growth for a single dendrite for different orientations by the PA method for the same PA-(A) random node arrangement $\theta_{def} = 0^{\circ}, 5^{\circ}, \ldots, 40^{\circ}, 45^{\circ}$

Thermal fluctuations. In order to avoid the symmetric shape of the dendrite in the conventional CA approach some fluctuations need to be introduced into the calculations. The following equation is commonly applied $P = 1 + \lambda^* rand$. Thermal noises are usually presented by putting the random fluctuations F into the calculations of latent heat, undercooling temperature or velocity [Voller (2008)]. It this paper we use then in the velocity calculations $V = V \times P$.

Neighborhood configuration. In the CA approach only the closest neighborhood configuration has been analyzed. Larger the value of R_H is chosen in the PA method more dendritic and irregular structures can be observed. A more extended area of neighbors needs to be taken into the consideration in the PA method. The radius of neighborhood should be kept at a minimum of 1.5 μm in case of $a = 0.5\mu$m. For smaller values the dendritic shapes become distorted and the preferred orientation is lost as well.

7.3 Simulated results

The dendritic morphologies were calculated by the classical FDM-CA and the novel FDM-PA approaches. The following numerical examples were prepared

- From CASE 1 to CASE 10 the dendritic growth process is simulated by the *PA method* with the same random node arrangement denoted (PA-(A)) for the following ten crystallographic orientations

  $\theta_{def} = 0^\circ, \quad \theta_{def} = 5^\circ, \quad \theta_{def} = 10^\circ, \quad \theta_{def} = 15^\circ, \quad \theta_{def} = 20^\circ,$

  $\theta_{def} = 25^\circ, \quad \theta_{def} = 30^\circ, \quad \theta_{def} = 35^\circ, \quad \theta_{def} = 40^\circ, \quad \theta_{def} = 45^\circ.$

- From CASE 11 to CASE 19 the dendritic growth process is simulated by the *PA method* with different random node arrangements (PA-(B), PA-(C), PA-(D)) for the following crystallographic orientations

  $\theta_{def} = 5^\circ, \quad \theta_{def} = 15^\circ, \quad \theta_{def} = 30^\circ.$

- From CASE 20 to CASE 25 the dendritic growth process is simulated by the *PA method* with different randomness of the node arrangement $\varepsilon = 0.10$, $\varepsilon = 0.25$ and $\varepsilon = 0.49$, for the following $\theta_{def} = 5^\circ$ and $\theta_{def} = 30^\circ$ crystallographic orientations.

- From CASE 25 to CASE 28 the dendritic growth process is simulated by the conventional *CA method* without and with random fluctuations.

- From CASE 29 to CASE 31 the dendritic growth process is simulated by the *PA method* including the factor responsible for the correction in the lengths of the x and y branches for different random node arrangements (PA-(B)-F, PA-(C)-F, PA-(D)-F).

The results have been arranged and represented in the following way. The FDM-PA calculations with different orientations of the crystallographic axis are depicted in Fig. 20 based on the same node arrangements. The lengths of the dendritic axes of these calculations are depicted in Fig. 19. Then Figs. 21,..,23 show the FDM-PA results with the varied random mesh structure for a single dendrite with $\theta_{def} = 5^\circ$, $\theta_{def} = 15^\circ$ and $\theta_{def} = 30^\circ$, respectively. The length of the dendritie axes of theses calculations are depicted in Fig. 24. Fig. 25. Fig. 26 represents dendritic growth for a single dendrite with $\theta_{def} = 5^\circ$ and $\theta_{def} = 30^\circ$ for a different node arrangement randomness. The simulations are shown for the conventional CA approach with and without random fluctuations in Fig. 27. Finally in Fig. 28 the results for the PA method, where the randomness correction factor is applied, are represented (see discussion in the next paragraph).

7.3.1 Discussion of the results

The orientations of crystallographic axes of different dendrites have different orientations in general. It is commonly recognized that this process is difficult to simulate by the classical CA method since the dendrite will always switch to 0° or 45° direction during the growth. Our testing is thus primarily focused on the growth of the dendrite at different orientations by the novel PA method. Simulated examples are for the random node arrangements PA-(A),..., PA-(F) presented in Fig. 20, and Figs. 21-23, respectively. They show that when employing the PA method any of the crystallographic orientations can easily be achieved. Results show that the proper growth direction is always observed with increasingly random ($\varepsilon \to 0.49$) node arrangement.

Finally, for the same input parameters the dendritic growth process was simulated by the CA and PA method for the $\theta_{def} = 0^\circ$ preferential crystallographic orientation (see CASE 1 and CASE 27, respectively). The lengths of x and y branches were different in both methods. This is due to the influence of the random node arrangement and subsequent variable distances between the nodes. In the CA method the same value of a is taken while for the PA method this distances are different and might vary between maximum $\Delta x = \Delta y = 2\varepsilon a$ and minimum $\Delta x = \Delta y = 2(1-\varepsilon)a$. It can be concluded that the differences in the length between x and y directions with respect to the random node arrangement are almost constant and kept below $\approx 5\%$. The standard deviation was calculated for the x and y lengths of the dendritic arms and for the ratio between them (see Fig. 19 and Fig. 24). The following features

can be summarized from Tab.3. The average length of the dendrite at ten different orientations and some random node arrangement with $\varepsilon = 0.49$ is 152.8 $\pm$ 5.18 μm. The average length of the dendrite calculated with four different random node arrangement for the fixed angles 5°, 15° and 30° is 153.37 $\pm$ 5.39 μm, 156.12 $\pm$ 6.44 μm and 151.75 $\pm$ 5.36 μm, respectively. From this one can conclude that the errors caused by the rotation of the dendrite are at the same order as the errors cussed by different random node arrangements. Fig.25 and Fig.26 demonstrate that when reducing ε from 0.49 to 0.1 the PA starts to behave like the CA and the proper simulation of the dendrite is not possible. We are too close to the classical node structure in such case and CA limitations appear.

To achieve the same dendrite length in PA method as in the CA method, an empirical factor, which multiplies the calculated velocity in the PA method, was added in the code. It can be shown that putting factor 1.25, (for the random node arrangement ε= 0.49) in the PA calculations, the branches will have the same length in both methods (see Fig. 28).

In the present study it is not necessary to put any thermal fluctuations in the PA method. The random node arrangements in the PA method replace the thermal fluctuations of the CA method.

Fig. 20 and Tab.3 show that the novel PA concept can be used to depict the dendritic growth process in any preferential orientation during the solidification process.

8 Conclusions

In this paper a novel PA method is developed and applied to modeling the dendritic growth process. Advantages of the developed PA method are

- No need for mesh generation or polygonisation. Only the node arrangement has to be generated, but without any geometrical connection between nodes.
- In the new PA method the governing equations are solved with respect to the location of points (not polygons) on the computational domain.
- The random grid PA method allows to rotate dendrites in any direction since it has a limited anisotropy of the node arrangements.
- PA method offers a simple and powerful approach of CA type simulations. It was shown that both methods are able to qualitatively and quantitatively model a diverse range of solidification phenomena in almost the same calculation time.

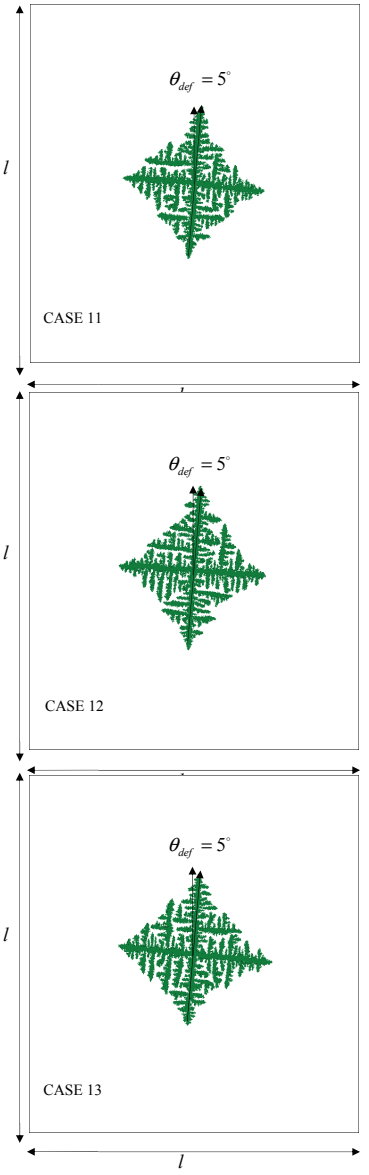

Figure 21: Simulated dendritic growth for a single dendrite with $\theta_{def} = 5^{\circ}$ for different random node arrangement structures: PA-(B), PA-(C), PA-(D), respectively

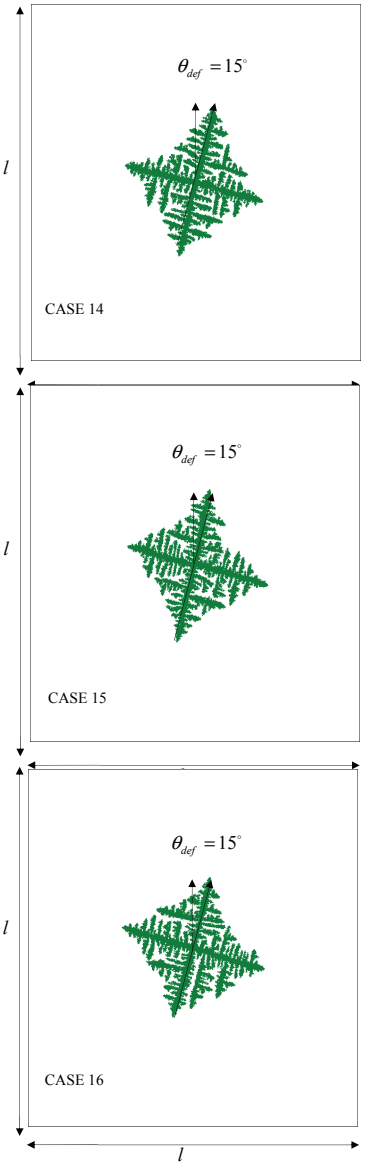

Figure 22: Simulated dendritic growth for a single dendrite with $\theta_{def} = 15^{\circ}$ for different random node arrangement structures: PA-(B), PA-(C), PA-(D), respectively

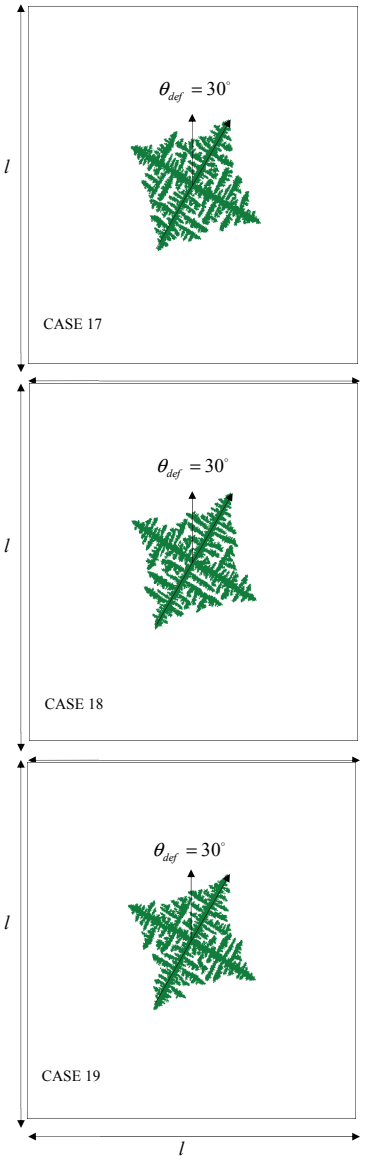

Figure 23: Simulated dendritic growth for a single dendrite with $\theta_{def} = 30^{\circ}$ for different random node arrangement structures: PA-(B), PA-(C), PA-(D), respectively

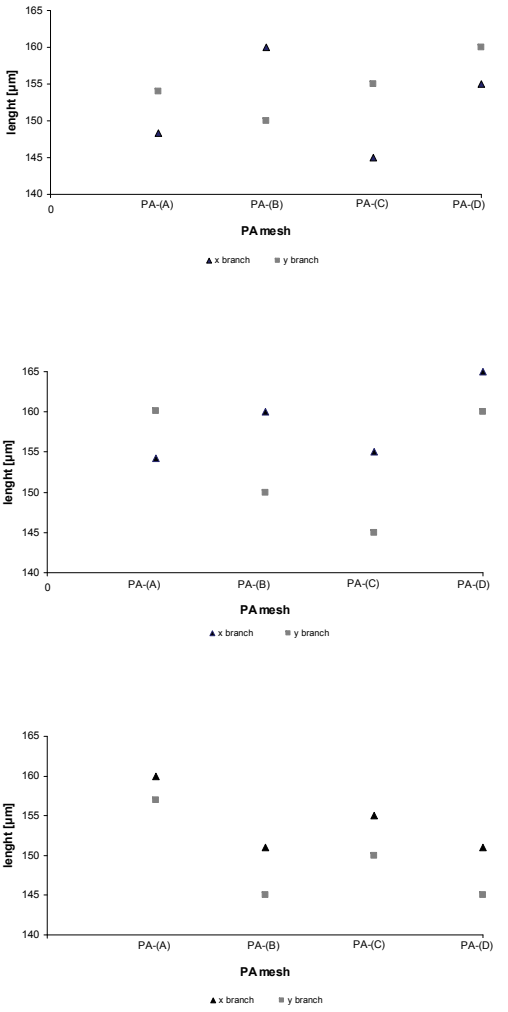

Figure 24: The lengths of the dendrite branches in x and y directions for the $\theta_{def} = 5^{\circ}$,$\theta_{def} = 15^{\circ}$ and $\theta_{def} = 30^{\circ}$ (from top to bottom) different orientations, for the random node arrangement (see Fig. 21, Fig. 22 and Fig. 23)

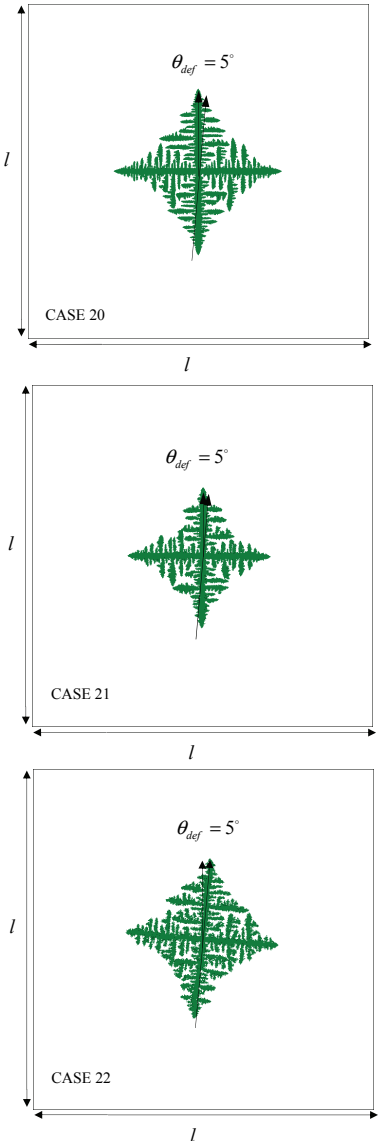

Figure 25: Simulated dendritic growth for a single dendrite with $\theta_{def} = 5^{\circ}$ for different node arrangement randomness $\varepsilon = 0.1$(PA-(E)), $\varepsilon = 0.25$(PA-(F)), $\varepsilon = 0.49$PA-(A) from the top to bottom

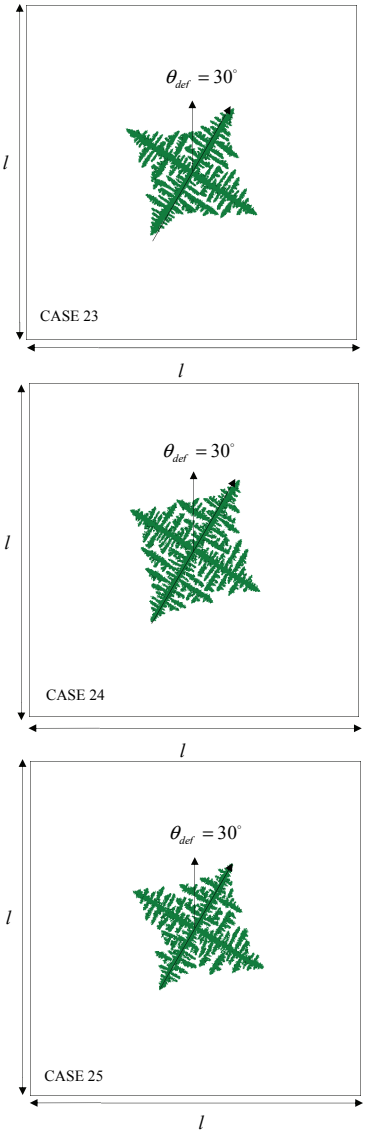

Figure 26: Simulated dendritic growth for a single dendrite with $\theta_{def} = 30^{\circ}$ for different node arrangement randomness $\varepsilon = 0.1$(PA-(E)), $\varepsilon = 0.25$(PA-(F)), $\varepsilon = 0.49$PA-(A) from the top to bottom

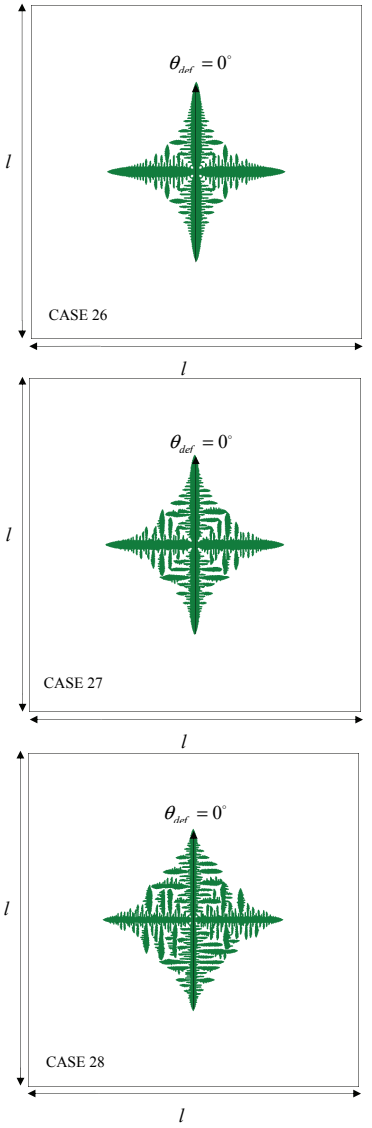

Figure 27: Simulated dendritic growth for a single dendrite for $\theta_{def} = 0^\circ$ by the CA method without $\lambda = 0$ (CASE 26) and with random fluctuations $\lambda = 0.05$ (CASE 27) and $\lambda = 0.3$(CASE 28), respectively

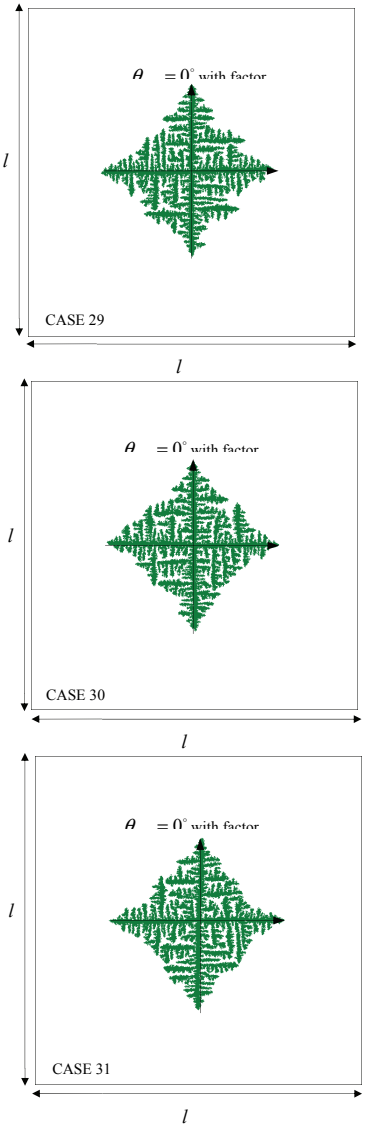

Figure 28: Simulated dendritic growth for a single dendrite for $\theta_{def} = 0^\circ$ by the PA method with factor 1.25 for the PA-(B)-F, PA-(C)-F, PA-(D)-F random node arrangement, respectively

Table 1: Nominal parameters used in the calculations

Symbol	Value	Unit
ρ	2700	kg/m^3
T_m	933.45	K
T_s	933.45-1.5	K
T_l	933.45+1.5	K
λ	210	W/mK
c_p	955.56	J/kgK
L	259259.26	J/kg
η	0.222	1
$\bar{\Gamma}$	1.6 x 10^{-7}	Km
δ_t	0.3	1
δ_k	0.75	1
S	4	1
R_c	1.5	μm
R_H	2	μm
μ_K	2	m/sK
l	350	μm
n	700	PA nodes/ CA cells
N	701	FDM nodes

- The dimension of the neighborhood radius and generation of the random node arrangement has to be chosen carefully in order to be able to rotate the dendrite.
- Straightforward node refinement possibility.
- Straightforward extension to 3-D.

The use of FDM-PA method instead of FDM-CA method implies transfer of the results from the regular FDM mesh to the irregular PA node arrangements and vice versa. This is not the case in the classical FDM-CA method. A replacement of the FDM method with a meshless [Atluri (2004); Liu and Gu (2005); Šarler, Vertnik and Perko (2005); Šarler and Vertnik (2006)] method that is able to directly cope with irregular node arrangement is underway.

Acknowledgement: The first author would like to thank the European Marie Curie Research Training Network INSPIRE for position to study and research at the University of Nova Gorica, Slovenia. The second author would like to thank

Table 2: Parameters used in the calculations

CASE	θ_{def}	λ^*	ε	node arangement
1	0°	0	0.49	PA-(A)
2	5°	0	0.49	PA-(A)
3	10°	0	0.49	PA-(A)
4	15°	0	0.49	PA-(A)
5	20°	0	0.49	PA-(A)
6	25°	0	0.49	PA-(A)
7	30°	0	0.49	PA-(A)
8	35°	0	0.49	PA-(A)
9	40°	0	0.49	PA-(A)
10	45°	0	0.49	PA-(A)
11	5°	0	0.49	PA-(B)
12	5°	0	0.49	PA-(C)
13	5°	0	0.49	PA-(D)
14	15°	0	0.49	PA-(B)
15	15°	0	0.49	PA-(C)
16	15°	0	0.49	PA-(D)
17	30°	0	0.49	PA-(B)
18	30°	0	0.49	PA-(C)
19	30°	0	0.49	PA-(D)
20	5°	0	0.10	PA-(E)
21	5°	0	0.25	PA-(F)
22	5°	0	0.49	PA-(A)
23	30°	0	0.10	PA-(E)
24	30°	0	0.25	PA-(F)
25	30°	0	0.49	PA-(A)
26	0°	0	0	CA
27	0°	0.05	0	CA
28	0°	0.3	0	CA
29	0°	0	0.49	PA-(B)-F
30	0°	0	0.49	PA-(C)-F
31	0°	0	0.49	PA-(D)-F

Table 3: The lengths of dendrite branches in x and y directions and related quantities with respect to the random node arrangement

results	method	x branch length [μm]	y branch length [μm]	ratio of primary dendrite arms x/y [-]	$\overline{x/y}$ average length ratio [-]	σ standard deviation of x/y [-]
					average length of $x$and$y$ [μm]	σ standard deviation of lenght [μm]
5°	PA-(A)	148.0	154.0	0.961	0.982	0.057
5°	PA-(B)	160.0	150.0	1.066		
5°	PA-(C)	145.0	155.0	0.935	153.37	5.39
5°	PA-(D)	155.0	160.0	0.968		
15°	PA-(A)	154.0	160.0	0.962	1.032	0.049
15°	PA-(B)	160.0	150.0	1.066		
15°	PA-(C)	155.0	145.0	1.068	156.12	6.44
15°	PA-(D)	165.0	160.0	1.031		
30°	PA-(A)	160.0	157.0	1.019	1.033	0.010
30°	PA-(B)	151.0	145.0	1.041		
30°	PA-(C)	155.0	150.0	1.033	151.75	5.36
30°	PA-(D)	151.0	145.0	1.041		
0°	PA-(A)	160.0	154.0	1.038		
5°	PA-(A)	148.0	154.0	0.961		
10°	PA-(A)	142.0	148.0	0.959	0.980	0.041
15°	PA-(A)	154.0	160.0	0.962		
20°	PA-(A)	160.0	148.0	1.081		
25°	PA-(A)	154.0	148.0	1.040		
30°	PA-(A)	160.0	157.0	1.019		
35°	PA-(A)	154.0	148.0	1.040	152.8	5.18
40°	PA-(A)	157.0	151.0	1.039		
45°	PA-(A)	151.0	148.0	1.020		

the Slovenian Research Agency for funding in the framework of the project J2-0099 Multiscale modelling of liquid-solid systems.

Reference

Atluri, S.N. (2004): *The Meshless Method (MLPG) for Domain and BIE Discretization,* Tech Science Press, Forsyth.

Anderson, M.P.; Srolovitz, D.J.; Grest, S.G. (1984): Computer simulation of grain growth. I. Kinetics. *Acta Metall*, vol.32, pp. 783-791.

Boettinger, W.J.; Coriell, S.R.; Greer, A.L.; Karma, A.; Kurz, A.; Rappaz, M.; Trivedi, R. (2000): Solidification microstructure recent developments, future directions. *Acta Metall.*, vol. 48, pp. 43-70.

Daming, L.; Ruo, L.; Zhang, P. (2004): A new coupled model for alloy solidification. *Science in China Ser. A. Mathermatics.*, vol. 47, pp. 41-52.

Gandin, Ch.A.; Rappaz, M. (1994): A coupled finite element-cellular automaton model for the prediction of dendritic grain structures in solidification processes. *Acta Metall.*, vol.42, no. 7, pp. 2133-2246.

Gandin, Ch.A.; Rappaz, M. (1997): A 3D cellular automaton algorithm for the prediction of dendritic grain growth. *Acta Metall.*, vol. 45, pp. 2187-2195.

Janssens, K.G.F. (2000): *Irregular cellular automata modeling of grain growth.* Continuum Scale Simulation of Engineering Materials, Germany.

Janssens, K.G.F. (2003): Random Grid, Three Dimensional, Space-Time Coupled Cellular Automata for the Simulation of Recrystallization and Grain Growth. *Mod. Sim. Mater. Sc.*, vol. 1, no. 2, pp.157-171.

Janssens, K.G.F.; Raabe, D.; Kozeschnik, E.; Miodownik, M.A.; Nestler, B. (2007): *Computational Materials Engineering*, Elsevier Academic Press, Great Britain.

Janssens, K.G.F. (2010): An introductory review of cellular automata modeling of moving grain boundaries in polycrystalline materials. *Mathematics and Computers in Simulations,* vol. 80, no. 7, pp. 1361-1381.

Krane, M.J.M.; Johnson, D.R.; Raghavan, S. (2009): The development of a cellular automaton - finite volume model for dendritic growth. *Applied Mathematical Modelling*, vol. 33, no. 5, pp. 2234-2247.

Kammer, K. (1999): *Aluminium Handbook1*. Aluminium-Verlag Marketing & Kommunikation GmbH.

Liu, G.R.; Gu, Y.T. (2005): *An Introduction to Meshfree Methods and Their Programming,* Springer, Dordrecht.

Lorbiecka, A.Z.; Vertnik, R., Gjerkeš, H.; Manojlović, G.; Senčič, B.; Cesar, J.; Šarler, B. (2009): Numerical modelling of Grain Structure in Continuous Casting of Steel. *CMC: Computers, Materials & Continua,* vol. 8, no. 3, pp. 195-208.

Lorbiecka, A.Z.; Šarler, B. (2009): Point automata method for prediction of grain structure in the continuous casting of steel. In: L. Andreas (ed) *3nd International Conference of Simulation and Modelling of Metallurgical Processes in Steelmaking, Steelsim 2009*, ASMET, Leoben, Austria, pp. 192-197.

Lorbiecka, A.Z.; Šarler, B. (2009): Modelling grain growth processes by the conventional Cellular Automata and New Point Automata method. In: G. Tsatsaronis and A. Boyano (ed) *International conference of Optimization Using Exergy- based Methods and Computational Fluid Dynamics*, Berlin, Germany, pp.243-252.

Lorbiecka, A.Z.; Šarler, B. (2010): A Sensitivity Study of Grain Growth Model For Prediction of ECT and CET Transformations in Continuous Casting of Steel. *Materials Science Forum*, vol. 649, pp. 373-378.

Midownik, M.A. (2002): A review of microstructural computer models used to simulate grain growth and recrystallisation in aluminium alloys. *J.Light. Met*, vol.2, no.3, pp. 125-135.

Nastac, L. (2004): *Modeling and Simulation of Microstructure Evolution in Solidifying Alloys*. Kluwer Academic Publishers.

Nakagawa, M.; Narsume, Y.; Ohsasa, K. (2006): Dendrite Growth Model Rusing Front Tracking Technique with New Growth Algorithm. *ISIJ International*, vol. 46, no.6, pp. 909-913.

Neumann, J.V. (1987): The general and logical theory of automata, 1963. In: W. Aspray and A. Burks, Editors, *Papers of John von Neumann on Computing and Computer Theory. The Charles Babbage Institute Reprint Series for the History of Computing,* vol. 12, pp. 477-490.

Rappaz, M.; Gandin, Ch.A. (1993): Probabilistic modeling of microstructure formation in solidification processes. *Acta Metall.*, vol.41, pp. 345-360.

Rettenmayr, M.; Buchmann, M. (2006): Solidification and Melting - Asymmetries and Consequences. *Materials Science Forum.*, vol.508, pp. 205-210.

Saito, Y.; Goldbeck-Wood, G.; Muller-Krumbhaar, H. (1988): Numerical simulation of dendritic growth. *Physical Review*, vol. 33, pp. 2148-2157.

Sasikumar, R.; Sreenivasan, R. (1994): Two-dimensional simulation of dendrite morphology. *Acta metall. mater*, vol. 42, no. 7, pp. 2381-2386.

Shin, Y.H.; Hong, C.P. (2002): Modeling of Dendritic Growth with Convection Using a Modified Cellular Automata Model with a Diffuse Interface. *ISIJ International*, vol. 42, no. 4, pp. 359-367.

Spittle, J.A.; Brown, S.G.R. (1989): Computer simulation of the effect of alloy variable on the grain structures of castings. *Acta. Metall.*, vol. 37, pp. 1803-1810.

Spittle, J.A.; Brown, S.G.R. (1995): A cellular automaton model of steady state columnar dendritic growth in binary alloys. *J.Mater. Sci*, vol. 30, pp. 3989-3994.

Stefanescu, D. M. (2009): *Science and Engineering of Casting Solidification*. Springer Science.

Šarler, B.; Vertnik, R.; Perko, J. (2005): Application of diffuse approximate method in convective diffusive solidification problems, *CMC: Computers & Materials, Continua,* vol. 2, pp. 77-83.

Šarler, B.; Vertnik, R. (2006): Meshfree local radial basis function collocation method for diffusion problems. *Computers and Mathematics with Application*, vol. 51, pp. 1269-1282.

Qin, R.S.; Wallach, E.R. (2003): A phase-field model coupled with a thermodynamic database. *Acta Materialia*, vol. 51, pp. 6199-6210.

Wolfram, S. (2002): *A New Kind of Science.* Wolfram Media, Inc.

Voller, V.R. (2008): An enthalpy method for modeling dendritic growth in a binary alloy. *Science Direct, International Journal of Heat and Mass Transfer*, vol. 52, pp. 823-834.

Xu, Q.; Li, B.; Liu, Y.; Liu, B. (2008): Numerical modelling of microstructure evolution and dendrite growth in alloy solidification process. *Int. J. Materials and Product Technology*, vol.33, pp. 37-49.

Xu, Q.Y.; Liu, B.C. (2001): Modeling of As-Cast Microstructure of Al Alloy with a Modified Cellular Automaton Method. *Materials Transactions*, vol. 42, no. 11, pp. 2316-2321.

Zhan, Z.; Wei, Y.; Dong, D. (2008): Cellular automaton simulation of grain growth with different orientation angles during solidification process. *Journal of Materials Processing Technology*, vol. 208, no. 1, pp. 1-8.

Zhu, M.F.; Hong, C.P. (2001): A modified cellular automaton model for the simulation of dendritic growth in solidification of alloys. *ISIJ International*, vol. 41, no. 5, pp. 436-445.